Control of Electronic Properties of Molecular Conductors by Uniaxial Strain

S. Kagoshima* and R. Kondo

Department of Basic Science, University of Tokyo, Komaba 3-8-1, Meguro-ku, Tokyo 153-8902, Japan

Received May 10, 2004

Contents

Seiichi Kagoshima was born in Osaka, Japan, and received a D.Sci. degree (1973) from the University of Tokyo. He has been a professor of physics at the Department of Basic Science, University of Tokyo, since 1979. His general research field is (experimental) condensed matter physics, with special interest in the electronic, magnetic, and structural properties of low-dimensional molecular conductors.

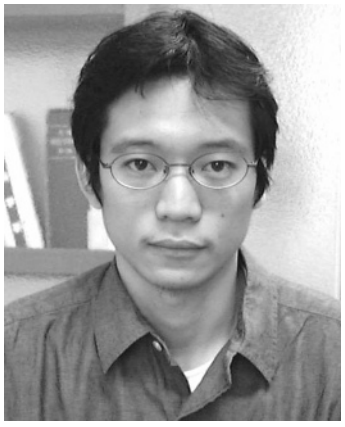

Ryusuke Kondo was born in Tokyo, Japan, and received a Ph.D. degree (2001) from the University of Tokyo. He has been a research associate at the Department of Basic Science, University of Tokyo, since 1998. His general research field is (experimental) condensed matter physics, with special interest in the development of new functional organic compounds and measurements of electronic properties and crystal structure analysis under extreme conditions (low temperature, high magnetic field, and high pressure).

1. Introduction: Roles of Pressure Application in the Study of Molecular Conductors

The application of hydrostatic pressure to molecular conductors provides a variety of electronic states such as metallic, superconducting, and magnetic and nonmagnetic insulating states.[1] Many phenomena of physical importance have been discovered, such as unconventional superconductivity, density waves, the Mott transition, and charge disproportionation. It is noteworthy that a monotonic increase in resistance with decreasing temperature, which had been observed in many molecular crystals, was found to be understood in terms of the Mott transition and charge disproportionation that are caused by Coulomb interaction between conduction electrons.[2−5]

The application of pressure to molecular crystals has been successful for two reasons: (1) softness of molecular crystals and (2) anisotropy in the electronic

* Author to whom correspondence should be addressed (telephone +81-3-5454-6737; fax +81-3-5454-4331; e-mail kagosima@mail.ecc.u-tokyo.ac.jp).

10.1021/cr0306539 CCC: $48.50
Published on Web 10/07/2004

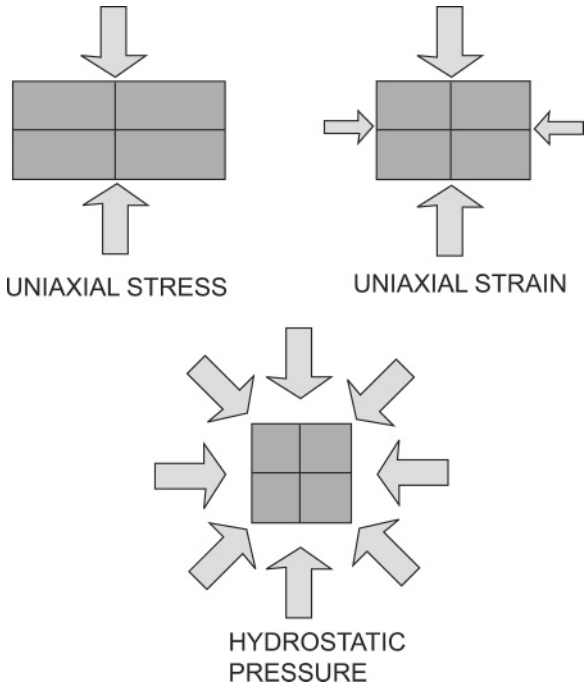

Figure 1. Compression of materials by various methods. Uniaxial stress causes Poisson's effect, which expands the material in the plane normal to the applied pressure.

structure. Softness is one of the characteristic properties of molecular conductors. Their elastic stiffness constant is smaller than those of conventional materials, such as popular semiconductors and ordinary metals, by an order of magnitude. Therefore, intermolecular or interatomic distances can be largely modified by moderate pressures to show dramatic changes in electronic properties. This characteristic is considered to be common to all molecular materials bonded by van der Waals force.

However, hydrostatic-pressure application has a flaw in that an isotropic pressure is applied to a sample. When the sample is isotropic in structure, it is compressed isotropically, as schematically shown in Figure 1. In anisotropic materials such as organic conductors, the sample suffers an anisotropic contraction, the anisotropy of which is inherent and cannot be controlled. If a phenomenon of interest is dominated by the overall volume effect, hydrostatic-pressure studies may provide precise knowledge about electronic states. In many molecular conductors, however, electronic properties are determined by not only the unit cell volume but also the molecular orientation and intermolecular distances along different directions. Therefore, it is crucial, in studies of molecular conductors, to learn which intermolecular interaction dominates which electronic properties.

Studies of uniaxial compression have been explored to elucidate the relationship between the crystal structure and electronic properties, by modifying the intermolecular or interatomic distance along a desired direction. In principle, the uniaxial compression (or elongation) is realized by applying a compressive (or stretching) force to a pair of parallel faces of a parallelepiped sample. However, this causes not only the compression (or elongation) along the intended direction but also expansion (or contraction) along transverse directions, as shown in Figure 1. This phenomenon is called Poisson's effect. The stress in the sample is uniaxial but the strain is not. Therefore, this experimental method is called the uniaxial *stress* method. Very recently, a uniaxial *strain* method was also developed, in which intermolecular distances can be modified along any desired direction with no appreciable changes in the transverse directions, as shown in Figure 1.

This paper is organized as follows: Section 2 is a brief review of the uniaxial stress method and its application to various materials. Section 3 and succeeding sections will be devoted to the development of the uniaxial strain method and its application to studies of the electronic properties of molecular conductors.

2. Uniaxial Stress Studies of Electronic Properties of Various Materials

2.1. Semiconductors and Oxides

The uniaxial stress method is popular in studies of semiconductors.[6−8] It is usually used for two purposes. One is the study of band parameters and their control by breaking the material's symmetry. For example, a crystal of cubic symmetry turns into a tetragonal one under uniaxial compression along one of the principal axes. This may allow an optical transition that is forbidden in the original cubic symmetry, leading to much knowledge about electronic states, possible excitons, and luminescence related to the transition. The other purpose of a uniaxial stress study is to clarify features of local strain (or deformation) in a crystal and to control them. For example, local electronic states around an impurity or a lattice defect in silicon may affect the characteristics of a semiconducting device. Quantum dots and thin epitaxial layers formed on a sheet of a semiconductor wafer usually involve local strains due to the heterostructure. An application of uniaxial stress can modify such local strains, leading to the control and improvement of electronic devices.

The uniaxial stress method was also applied to studies of the mechanism of the high-transition-temperature (high-T_c) superconductivity.[9−12] It occurs usually in a very anisotropic layered structure of oxides. The uniaxial compression was applied along the direction perpendicular to a conducting plane or along one of the axes in the conducting plane to elucidate the roles of the interatomic distance along various directions in the superconductivity. Some enhancement of superconductivity, for example, $d\ln T_c/dP \simeq 0.02$ GPa^{-1},[9] has even been discovered in such investigations.

There are three ways of applying uniaxial stress. One is direct compression of a bulk sample by a piston or an anvil. Another is direct stretching of a needlelike sample by holding its ends. The third is indirect compression or elongation of a thin sample glued onto a bulk plate that is bent by applying an external force.

The piston or anvil method is the most popular among the three methods. In the piston method, the

maximum stress reached is usually 1 GPa (10 kbar) or less because of sample fracture or possible breakage of apparatuses. Optical, X-ray, and neutron measurements can be made in addition to electrical measurements.[6] Besides the piston, a pair of diamond anvils for hydrostatic-pressure studies has been employed to apply uniaxial stress of 5−10 GPa to a semiconductor having four electrical leads for resistance measurements.[13] Even a conventional set of diamond anvils having a gasket and a liquid pressure medium such as alcohol can be used to apply the uniaxial stress at low temperature.[14] The alcohol, which is frozen at low temperatures, serves as a plastic plate inserted between the diamond anvil and the sample to ensure close contact between them.

Stretching of a needlelike sample creates a negative uniaxial stress. One of the difficulties of this method is how to hold the two ends of the sample. Glue is used to attach the sample ends to mechanical parts of the apparatus to pull the sample. This method has been applied to studies of conventional semiconductors and two molecular superconductors, as described in the next section.

2.2. Molecular Conductors

Softness of a molecular material makes it easy to create a large deformation in a sample by applying a relatively small external force. Therefore, the application of pressure, be it hydrostatic or uniaxial, can be regarded not only as a structural perturbation to a sample but also as another method of creating materials having *new structures*.

The elongation method to stretch needlelike materials was applied to the first polymeric superconductor $(SN)_x$ with the critical temperature T_c of about 0.3 K to study roles of three-dimensional nature in dominating electrical conduction in the metallic state.[15−17] Bouffard et al. conducted pioneering work on applying the uniaxial stress to tetrathiofulvalene−tetracyanoquinodimethane (TTF-TCNQ), the most famous, first organic compound showing highly metallic properties, to clarify the relationship between intermolecular distance along three crystallographic axes and the anisotropy in electrical resistivity.[18] They employed the method of indirect elongation of a sample glued onto a beam bent by an external force. By analyzing the obtained results, they discussed the relationship between mechanisms of the metallic conduction along the one-dimensional axis and the diffusive one along the transverse axes.

Tokumoto et al.[19] and Kusuhara et al.[20] conducted work on applying the uniaxial stress to organic superconductors to modify the superconducting transition temperature T_c. The former employed the piston method to apply the uniaxial (compressive) stress of about 1 MPa (10 bar) to κ-(BEDT-TTF)$_2$Cu(NCS)$_2$, where BEDT-TTF denotes bisethylenedithiotetrathiafulvalene, and found a small decrease in T_c. They selected samples that have a good shape conducive to compression by the piston. The latter developed a unique method of stretching a long sample of κ-(BEDT-TTF)$_2$Cu(NCS)$_2$. They glued the two ends of the sample to a frame of aluminum using epoxy. The sample suffers an effective stretch along one of the axes in its conducting layer with decreasing temperature because thermal contraction of the sample is greater than that of the aluminum frame. They observed an increase in T_c of 0.5−2 K.

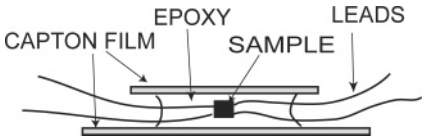

Figure 2. Encasement of a sample in epoxy resin for electrical resistance measurements.

One of the flaws of molecular materials is mechanical fragility and weakness against heating and organic solvent. This makes it difficult to apply the high pressures necessary to cause a measurable change in the sample. In addition, the shape of as-grown samples restricts the direction of stress application. Campos et al. developed a novel experimental method, the epoxy method, to overcome the above difficulties.[21] They encased a sample in epoxy resin, DuPont's Stycast 1266, that can be polymerized at room temperature, as shown in Figure 2. The piston safely compressed the sample−epoxy composite even at low temperatures. The merit of this method is the similarity of elastic properties between the sample and epoxy. This ensures the similarity of deformation in the sample and the epoxy, leading to protection of the sample from mechanical fracture. They investigated the effects of stress applied perpendicular to the conducting plane of α-(BEDT-TTF)$_2$NH$_4$Hg(SCN)$_4$ and found an increase in T_c and the inducement of superconductivity in α-(BEDT-TTF)$_2$KHg(SCN)$_4$.

The uniaxial stress method described in this section is useful enough to study the properties of materials having high symmetry because Poisson's effect, which changes the intermolecular distance in the transverse direction, does not seriously affect the interpretation of experimental results. However, in the studies of anisotropic materials such as molecular conductors, the uniaxial stress method encounters a difficulty. For example, a layered material compressed or elongated by the uniaxial stress method along an axis in the layer suffers Poisson's effect along both the other axis in the layer and the third axis perpendicular to the layer. The effects are usually different in magnitude from each other, and their roles in dominating electronic properties must also be different. Therefore, it is difficult to determine which elongation [intralayer or interlayer intermolecular (or interatomic) distance] is related to the observed changes in electronic properties under uniaxial stress. For example, Kusuhara et al., as mentioned above, encountered an ambiguity in interpreting their results because of this problem. To overcome this difficulty, it is desirable to control the intermolecular or interatomic distance along a desired direction without any change in other directions. The uniaxial *strain* method was thus developed, as described in the following sections.

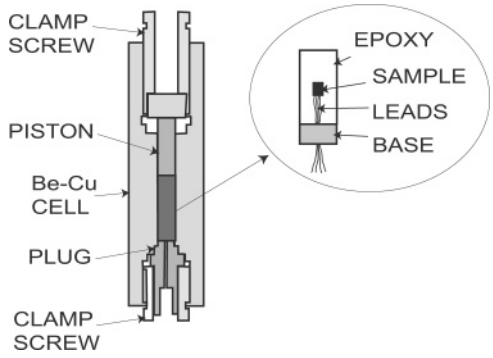

Figure 3. Uniaxial strain cell for electrical resistance measurements.

3. Development of Uniaxial Strain Method

3.1. Apparatuses for Electrical Resistance Measurements

In principle, Poisson's effect accompanying the application of uniaxial stress can be suppressed when a hard cylinder surrounds the side face of a sample. For studies of molecular materials, which are fragile and have irregular shapes, the epoxy method must be employed. Thus, the apparatus depicted in Figure 3 was developed to induce uniaxial strain in molecular conductors without Poisson's effect.[22] As the epoxy, Stycast 1266 was employed, as Campos et al. did. The deformation of the sample−epoxy composite would be purely uniaxial, because Young's modulus of Be−Cu, of the order of 10^{11} N/m^2 or more, is sufficiently large compared with that of epoxy (and also many other organic solids), the Young's modulus of which is of the order of 10^{10} N/m^2 or less. Poisson's effect in the epoxy is expected to be suppressed by the hard cell of Be−Cu. If the elastic constant of the sample is similar to that of epoxy, the deformation of the sample would be similar to the deformation of the sample−epoxy composite and would lead to the creation of uniaxial strain in the sample. Young's modulus of the most precisely studied organic conductor, TTF-TCNQ, has been evaluated to be about 1×10^{10} N/m^2 along the one-dimensional axis at room temperature.[23] This suggests that the uniaxial strain method described here creates a rather ideal uniaxial strain in crystals of molecular conductors.

Polymerization procedures sometimes deteriorate the sample due to chemical reaction between, presumably, the catalyst used for polymerization and the sample (or glue for attaching electrical leads to the sample). Two methods enabled this problem to be overcome: coating the sample with some paint such as General Electric varnish 7031, or encasing the sample in epoxy just before the liquid epoxy began to solidify.

Organic solids other than epoxy may be used to encase a sample. For example, Young's modulus values of nylon and polystyrene are about one-third of that of epoxy. They can be used for samples softer than TTF-TCNQ. It is noted, however, that one should encase a sample in organic solids without heating because many molecular conductors are damaged at temperatures higher than, for example, 50 °C. It was found that any oil used for conventional hydrostatic-pressure studies could be used to encase a sample in the uniaxial strain method. The setup is same as that for hydrostatic-pressure studies. The only difference is that the cell with the sample is first cooled to low temperatures at ambient pressure to freeze the oil, and then the piston of the cell is depressed via a long stainless steel rod from outside the cryostat. This method was called the frozen-oil method. Figure 4 shows the schematic view of the rod for depressing the piston. Three short rods were screwed together with a sheet of epoxy between rods to reduce heat input. Sheaths of Teflon were wrapped around the rods to reduce the possible friction between the rods and the stainless steel pipe. Needless to say, the magnitude of compression can be controlled during measurements.

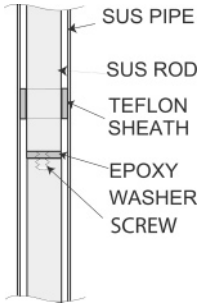

Figure 4. Stainless steel rod to depress the piston of the pressure cell.

When the uniaxial strain is created at room temperature followed by measurements at low temperature, one must be careful about thermal contraction of the sample, pressure medium, and pressure cell to ensure the existence of uniaxial strain at low temperature. X-ray measurements, the details of which will be described below, at low temperature have verified that the uniaxial strain created at room temperature is still present at low temperature if the magnitude of strain at room temperature is higher than a threshold.

Measurements of electrical resistance and thermopower were made by encasing an ordinary set of sample and electrical leads, as shown in Figure 3. The feed-through for electrical leads need not be very tight because the pressure medium in the cell is not liquid but solid. The epoxy method makes it possible to rotate the clamped cell to study, for example, magnetic field effects on electronic properties of the sample. The frozen-oil method has the advantage that a sample can be used in many experimental runs because the sample can be taken out of the liquid oil at room temperature without any damage to the sample.

3.2. Apparatuses for X-ray Structural Analysis

Lattice parameters and atomic positions of uniaxially strained crystals must be determined by X-ray diffraction, because most crystals of molecular conductors have low symmetry, such as $P1$ and $P\bar{1}$, and it is not straightforward to predict atomic displacements due to the uniaxial strain. To measure X-ray diffraction under uniaxial strain, the pressure cell shown in Figure 5 was designed. The Be−Cu cylinder employed in electrical measurements was replaced

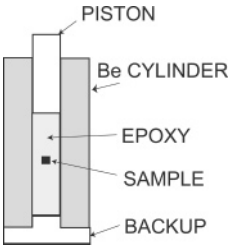

Figure 5. Uniaxial strain cell for X-ray diffraction measurements.

with a Be tube and a supporting shell of Be−Cu to ensure high transmission of Mo Kα X-rays. About 80% of Mo Kα X-rays can pass through the Be tube with a wall thickness of 4 mm in total. Direct measurements showed that 85% of Mo Kα X-rays passed through the epoxy rod of of 2 mm diameter. It was possible to apply piston pressures as high as 1 GPa (10 kbar) to the sample−epoxy rod in the Be tube. Higher pressures caused the Be tube to break. Considering Poisson's effect in ordinary materials, it is suggested that this piston pressure, 1 GPa (10 kbar), presumably causes a pressure of about 0.5 GPa (5 kbar) or less at the inner face of the Be tube.

As is often done in X-ray measurements with a diamond anvil cell, the goniometer was controlled by taking into account angular restriction by the window of the Be−Cu shell. Absorption corrections were made against X-ray beams passing diagonally through the Be tube and the sample−epoxy rod.

X-ray measurements at low temperature were made by setting the pressure cell on a cold stage of a cryostat. The pressure cell was cooled by conduction to have a minimum temperature as low as 6 K.

4. Uniaxial Strain Studies of Electronic Properties of Molecular Conductors

Uniaxial strain studies have been carried out mostly on BEDT-TTF-based molecular conductors, such as α-(BEDT-TTF)$_2$KHg(SCN)$_4$, in which molecules have a layered structure and a quasi-two-dimensional nature of the electrical properties. One exception is the first organic superconductor, (TMTSF)$_2$PF$_6$, which has a stack-columnar structure of tetramethyltetraselenafulvalene (TMTSF) and quasi-one-dimensional electrical properties. In section 4.1, we will describe several examples of modifying the band structure to find novel electronic properties in metallic phases under uniaxial strain. Examples of controlling the electron−electron Coulomb interactions that play important roles in stabilizing insulating states and, possibly, superconductivity, are shown in section 4.2.

4.1. Control of the Band Structure

4.1.1. Electrical and X-ray Structural Studies of α-(BEDT-TTF)$_2$XHg(SCN)$_4$

It was found that one can modify and control the band structure to stabilize the metallic, superconducting, or density-wave state, due to the electronic low-dimensional nature of α-(BEDT-TTF)$_2$XHg(SCN)$_4$, where X = K and NH$_4$, by changing the direction and magnitude of uniaxial strain. Figure 6 shows the crystal structure of α-(BEDT-TTF)$_2$XHg(SCN)$_4$ (X = K, NH$_4$), and Figure 7 denotes the arrangement of BEDT-TTF molecules in the conducting layer viewed along the molecular long axis.[24] The BEDT-TTF molecules form columns parallel to the *c*-axis, and the parallel arrangement of those columns provides a plane for the two-dimensional motion of conduction electrons. The band structure calculation based on the extended Hückel and the tight-binding approxi-

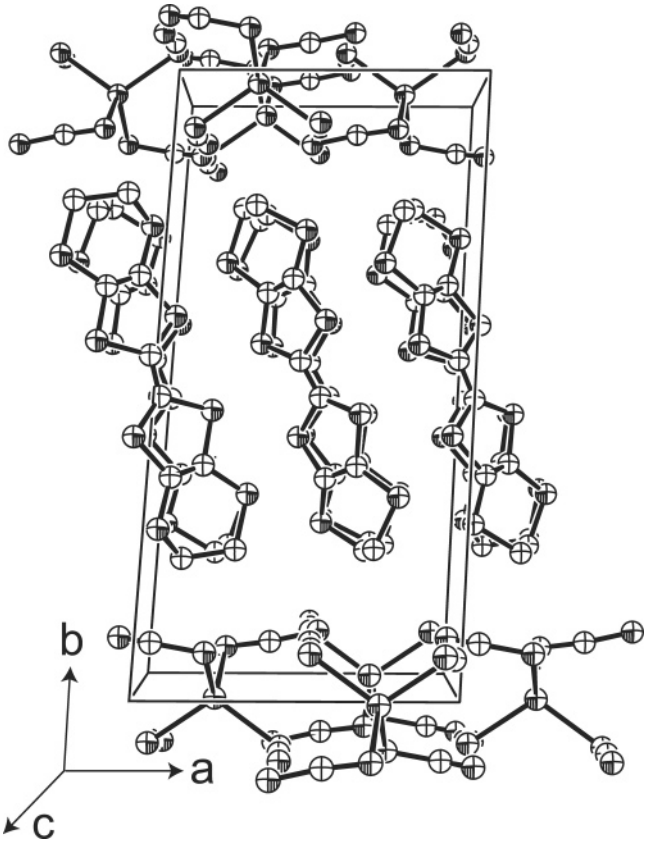

Figure 6. Crystal structure of α-(BEDT-TTF)$_2$NH$_4$Hg(SCN)$_4$.[24]

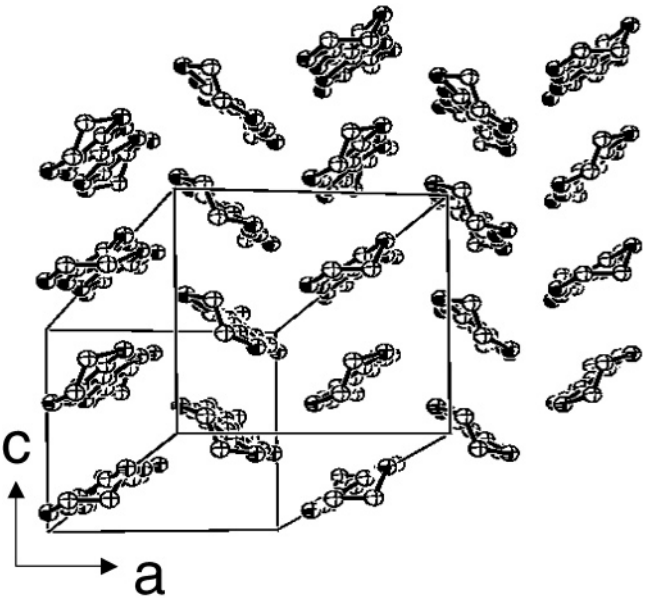

Figure 7. Arrangement of BEDT-TTF molecule in the conducting layer of α-(BEDT-TTF)$_2$NH$_4$Hg(SCN)$_4$.[24]

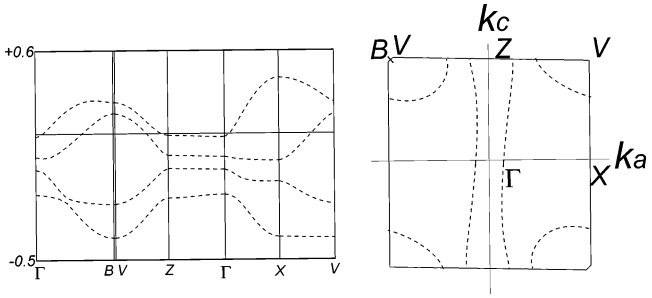

Figure 8. Band dispersion and the Fermi surface of α-(BEDT-TTF)$_2$NH$_4$Hg(SCN)$_4$ at ambient pressure.[24,25]

mation has given the band dispersion and the Fermi surface, as shown in Figure 8.[24,25] The Fermi surface is composed of a pair of sheetlike surfaces and an elliptical cylinder. The former suggests the presence of a one-dimensional metallic nature and the latter, a two-dimensional metallic one. At ambient pressure, the NH_4 compound shows metallic behavior with decreasing temperature followed by the onset of superconductivity at about 1 K.[26,27] The superconducting critical temperature T_c was found to decrease with increasing hydrostatic pressure. The K compound also shows metallic behavior with a small anomaly at about 8 K, but shows no superconductivity in the lower temperature range.[28−30] The anomaly at 8 K has been ascribed to a reconstruction of the band structure due to an instability characteristic of the one-dimensional electronic system, as suggested by the sheetlike Fermi surface.[31,32] Hydrostatic pressure suppresses the anomaly at 8 K, leading to a simple metallic state without superconductivity.[33]

The generation of uniaxial strain in NH_4 and K compounds changes the temperature dependence of electrical resistance, as shown in Figures 9 and 10.[34−36] The resistance was measured perpendicular to the conducting plane, the *ac* plane, according to the conventional dc four-lead method. The uniaxial strain was generated by using the frozen-oil method.

The uniaxial strain parallel to the *c*-axis enhanced the superconducting transition temperature T_c of the NH_4 compound to about 6 K under the piston pressure of 0.5 GPa (5 kbar). This gives the pressure derivative $d\ln T_c/dP$ of about 8 GPa^{-1}. It is surprising that such a large increase in T_c was caused by compressing superconducting materials because pressure application has been usually believed to reduce T_c. For example, the pressure derivative was evaluated to be −0.5 GPa^{-1} for (TMTSF)$_2$X,[37−39] −1.2 GPa^{-1} for β-(BEDT-TTF)$_2$I$_3$,[40,41] and −1.3 GPa^{-1} for κ-(BEDT-TTF)$_2$Cu(NCS)$_2$.[42] Some oxide superconductors showed increases of T_c with pressure, but their pressure derivative was of the order of 0.1 GPa^{-1}.[43] Also, the uniaxial stress study found an increase with the pressure derivative of only 0.02 GPa^{-1}.[9]

On the other hand, uniaxial strain parallel to the *a*-axis easily suppressed the superconductivity. The piston pressure of 0.45 GPa (4.5 kbar) induced an anomaly in resistance at about 8 K reminiscent of that observed in the K compound at ambient pressure. It was verified by angle-dependent magnetoresistance measurements (AMR) that this anomaly had exactly the same origin as that of the K compound, which is the change in the geometry of the Fermi surface. (AMR can be used to investigate the geometry of the Fermi surface of conducting electrons.[44]) Under greater strain, the sample showed simple metallic behavior.

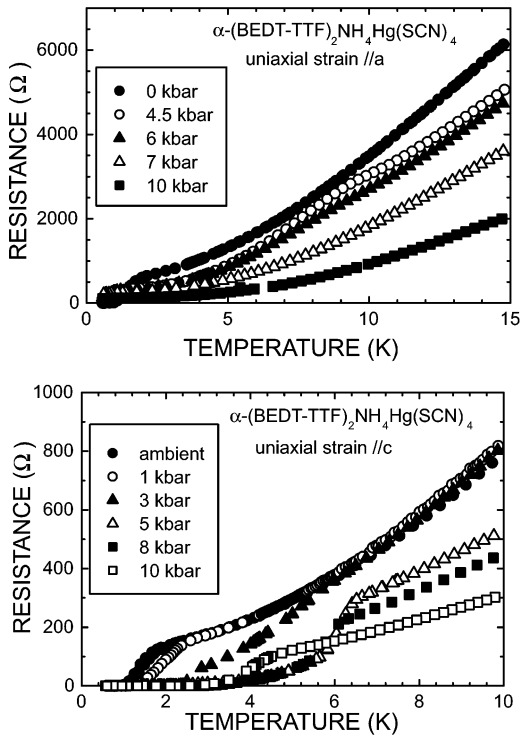

Figure 9. Temperature dependence of the electrical resistance of α-(BEDT-TTF)$_2$NH$_4$Hg(SCN)$_4$ under uniaxial strain.[34−36]

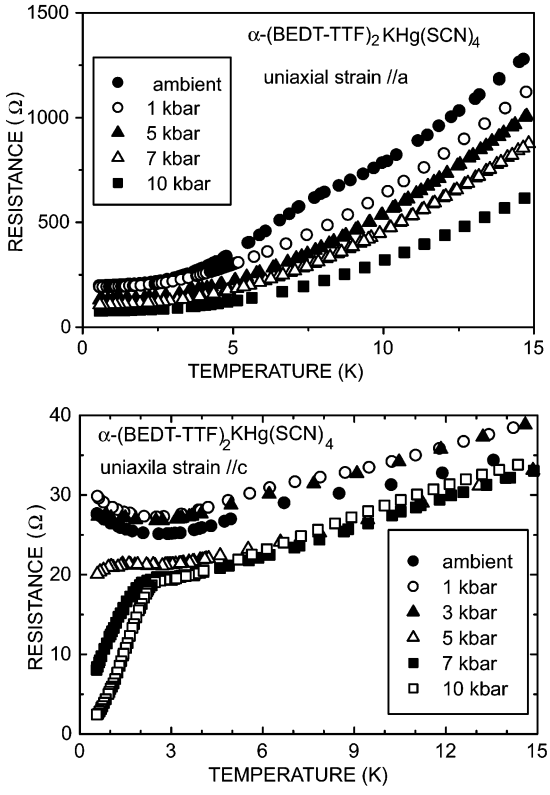

Figure 10. Temperature dependence of the electrical resistance of α-(BEDT-TTF)$_2$KHg(SCN)$_4$ under uniaxial strain.[34−36]

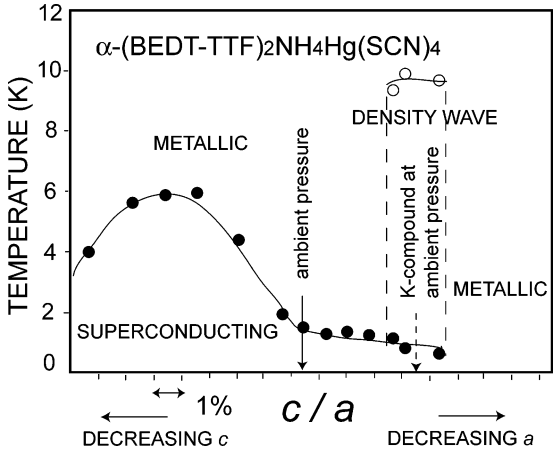

Figure 11. Phase diagram of α-(BEDT-TTF)$_2$NH$_4$Hg(SCN)$_4$ for the control of the lattice parameter ratio *c*/*a*. Curves are guides for the eye. α-(BEDT-TTF)$_2$KHg(SCN)$_4$ was considered to be located as shown by the arrow.[34,36,45]

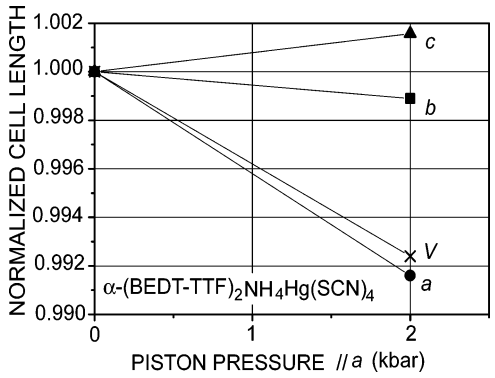

Figure 12. Change in the lattice parameters of α-(BEDT-TTF)$_2$NH$_4$Hg(SCN)$_4$ under the uniaxial strain parallel to the *a*-axis. (Reprinted with permission from ref 46. Copyright 2001 Elsevier Science.)

In the K compound, the uniaxial strain generated by the piston pressure of 0.3−0.4 GPa (3−4 kbar) parallel to the *c*-axis suppressed the resistance anomaly, as shown in Figure 10, and stabilized the simple metallic state. The piston pressure of 1 GPa (10 kbar) induced superconductivity. In both K and NH_4 compounds, the uniaxial strain perpendicular to the conducting *ac* plane gave results similar to those under the *c*-axial strain, although the effects were weaker. It is expected that the in-plane strain plays a dominant role in determining the electronic properties.

These results suggested the phase diagram depicted in Figure 11.[34,36,45] It was conjectured that the K and NH_4 compounds at ambient pressure were located on the phase diagram, as shown in the figure, and that their positions were shifted by the uniaxial strain parallel to the *a*- or *c*-axis, leading to the changes in electronic properties observed in resistance measurements.

The above conjecture should be checked by band calculations based on X-ray structure analyses. Such calculations have been carried out for the NH_4 compound.[46,47] First, lattice parameters were measured at room temperature under uniaxial strain. Figures 12 and 13 show examples of the results for the uniaxial strain in the conducting plane. In both

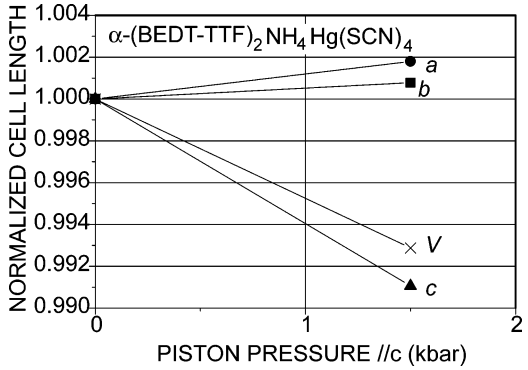

Figure 13. Change in the lattice parameters of α-(BEDT-TTF)$_2$NH$_4$Hg(SCN)$_4$ under the uniaxial strain parallel to the *c*-axis. (Reprinted with permission from ref 46. Copyright 2001 Elsevier Science.)

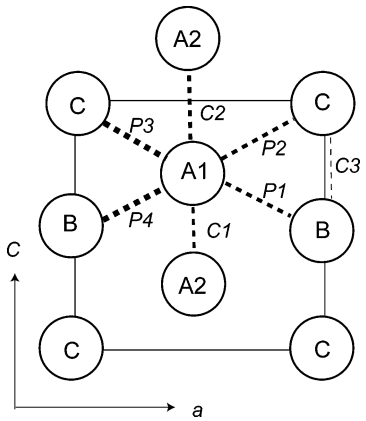

Figure 14. Important overlap integrals in the conducting layer of α-(BEDT-TTF)$_2$NH$_4$Hg(SCN)$_4$.

cases, the volume decreased by about 0.8% at about 0.2 GPa (2 kbar), but the *a*- and *c*-axes were selectively compressed under the uniaxial strains parallel to the respective axes. It is evident that these compressions created rather ideal uniaxial strains in the lattice. However, the compression parallel to the *b**-axis, which is normal to the conducting *ac*-plane, caused an appreciable decrease of the parameter *c*. This negative Poisson's effect is presumably due to a mismatch of the elastic constants between epoxy and the sample parallel to the *c*-axis.

Atomic coordinates were also deduced from the X-ray measurements. Under uniaxial strain, some changes were noted in the geometry between neighboring molecules. These changes were examined from the viewpoint of overlap integrals, regarding the shape of a BEDT-TTF molecule to be a rectangle formed by sulfur atoms on the outer six-member rings. Figure 14 shows important overlap integrals. It was found that the molecular distance dominated the overlap integrals of the intracolumnar group (C group), and the dihedral angle and the angle between the long axes dominated those of the intercolumnar one (P group).

For the intracolumnar C group, the overlap integrals increased with decreasing distance. Under the strain parallel to the *a*-axis, the distance for *C*1 increased and those for *C*2 and *C*3 decreased, leading to the results in Table 1.

With the strain parallel to the *b**-axis, which is perpendicular to the conducting plane, the distance

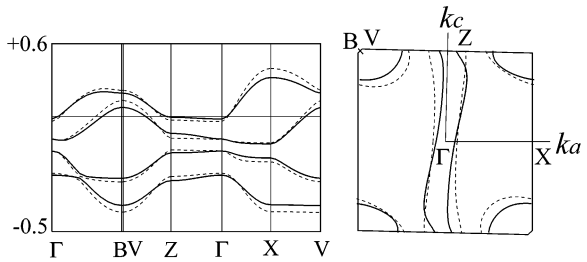

Figure 15. Band dispersion and the Fermi surface of α-(BEDT-TTF)$_2$NH$_4$Hg(SCN)$_4$ under the uniaxial strain parallel to the *c*-axis. The dashed curves denote those at ambient pressure.[46,47]

Table 1. Calculated Overlap Integrals ($\times 10^{-3}$) under Each Conditon of Uniaxial Compression[46,47]

		ambient	*a*-0.2GPa	*b**-0.1GPa	*c*-0.15GPa
intracolumnar	*C*1	−2.4	−2.0	−1.8	−3.6
	*C*2	6.0	6.6	8.8	7.2
	*C*3	−0.7	−1.1	−1.0	−1.1
intercolumnar	*P*1	−8.7	−9.3	−8.4	−7.3
	*P*2	−9.5	−10.0	−6.3	−7.6
	*P*3	13.6	14.1	12.1	13.3
	*P*4	13.4	13.0	12.7	12.5

for *C*1 increased and that for *C*3 decreased, the same as with the *a*-axial strain. Concerning *C*2, the strain reduced the intermolecular distance between the A1 and A2 molecules and increased the shift of the A1 molecule relative to the A2 one along the molecular long axis. This is expected to contribute to the increase of *C*2. The presence of vacancies in the anion layer above the A1 molecule and below the A2 one is considered to drive such molecular movements. Under the *c*-axial strain, the external force is along the intracolumnar group, causing the decrease of the distance and the increase of the overlap integral.

For the intercolumnar group, the overlap integrals increased with decreasing dihedral angle and decreasing angle between the long axes; that is, the molecules become almost parallel to each other.

Calculation of the band structure based on the obtained atomic coordinates revealed the following:[47] (1) At ambient pressure, the electronic properties have both one- and two-dimensional natures as described already. The uniaxial strain parallel to the *a*-axis enhanced the one-dimensional nature. This is consistent with the electrical properties that showed a resistance anomaly at about 8 K, suggesting the onset of an electronic instability characteristic of the one-dimensional electronic system. (2) As shown in Figure 15, the uniaxial strain parallel to the *c*-axis reduced the bandwidth and weakened the one-dimensional nature, as suggested by the more warped Fermi surface running parallel to the k_c-axis. These changes enhance the electronic density of states at the Fermi level. These are considered to be favorable for the enhancement of superconductivity because the instability due to the one-dimensional nature is suppressed and T_c predicted by the BCS theory for superconductivity increases with the increasing density of states. The increase of T_c to 6K was found to be semiquantitatively consistent with this theoretical prediction.[47] (3) The uniaxial strain parallel to the *a*-axis enhanced the one-dimensional nature, which was considered to be favorable for the onset of the density wave state.

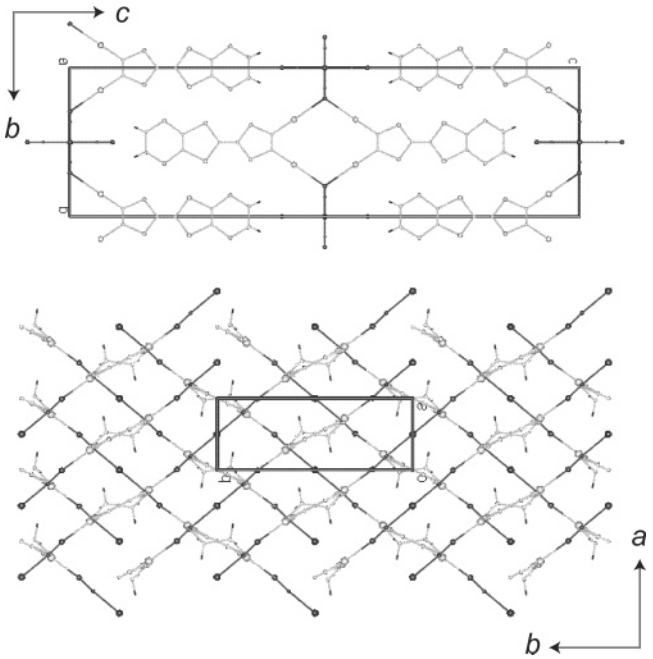

Figure 16. Crystal structure of θ-(DIETS)$_2$[Au(CN)$_4$] viewed along the conducting layer (upper figure) and that along the molecular long axis (lower one).[49,50]

A band structure of the K and NH$_4$ compounds at ambient pressure has been calculated.[48] Comparison of Fermi surfaces of these compounds suggested that the K compound had a more one-dimensional nature, which could explain the presence and absence of the density-wave state in the K and NH$_4$ compounds, respectively. This conjecture was directly verified by the uniaxial strain study.

Thus, it was found that the changes in the electronic properties of α-(BEDT-TTF)$_2$XHg(SCN)$_4$ (X = K, NH$_4$) caused by uniaxial strain were well explained by the changes in the band structure derived from the crystal structure under the uniaxial strain.

4.1.2. Electrical Measurements of Other Types of Molecular Conductors: θ-(DIETS)$_2$[Au(CN)$_4$] and (TMTSF)$_2$PF$_6$

a. θ-(DIETS)$_2$[Au(CN)$_4$]. A supramolecular conductor, θ-(DIETS)$_2$[Au(CN)$_4$], where DIETS denotes diiodo(ethylenedithio)diselenadithiafulvalene, based on iodine bonding, was synthesized to show superconductivity at 8.6 K under uniaxial strain created by the piston pressure of 1 GPa (10 kbar).[49,50] Figure 16 shows a schematic view of the crystal structure at ambient pressure. DIETS is an asymmetrical molecule containing two iodine atoms on one of the edges of the skeleton.

In recent progress of supermolecular chemistry, the halogen-based intermolecular interactions have been attracting much attention for the design and control of crystal structures of molecular conductors.[51] Among halogen atoms, the iodine atom has the following remarkable features: (1) its introduction to TTF family donors does not harm the intrinsic donor ability because of the small electronegativity of the iodine atom, and (2) a strong and directional interac-

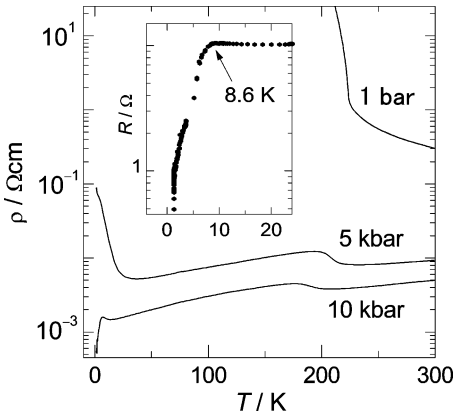

Figure 17. Electrical resistance of θ-$(DIETS)_2[Au(CN)_4]$ under the uniaxial strain perpendicular to the conducting plane. (Reprinted with permission from ref 49. Copyright 2002 The Royal Society of Chemistry.)

tion exists between the iodine atom of the TTF family donor and a lone pair on the nitrogen atom, because the lowest unoccupied molecular orbital (LUMO) of the donor is strongly localized on the iodine atom. This strong I−N interaction was named an "iodine bond" by Imakubo et al.,[49] who reported several unique crystal structures of supramolecular organic conductors based on the iodine bond.[52]

θ-$(DIETS)_2[Au(CN)_4]$ has the iodine bond, that is, the I−N contact, the distance (3.02 Å) of which is shorter than the sum of the van der Waals radii (3.53 Å) of the iodine atom of DIETS and the nitrogen one of the metal−cyanate anion. It is interesting to see the possible roles of the iodine bond in dominating electronic properties of organic conductors.

Figure 17 shows the temperature dependence of the electrical resistivity of θ-$(DIETS)_2[Au(CN)_4]$ measured perpendicular to the conducting ab-plane at ambient pressure and with the uniaxial strain perpendicular to the conducting plane. At ambient pressure, there is a rapid increase in resistivity at about 225 K. Hydrostatic-pressure application suppressed the resistance increase but did not stabilize the metallic state. It was found, however, that the uniaxial strain perpendicular to the conducting plane suppressed the insulating behavior and induced superconductivity at about 8.6 K, as shown in Figure 17. Such behavior was not observed under the uniaxial strain along other directions. Although the exact role of the iodine bond is not clear at present, the high anisotropy of the pressure effect upon the electrical conductivity suggests some kind of relationship between the iodine bond and the electronic state at low temperature.

It has been conjectured that the bandwidth in the conducting plane is increased by the uniaxial strain perpendicular to the conducting plane, leading to the metallic state where superconductivity can occur.[53] The crystal structure shown in Figure 16 supports this idea because DIETS molecules aligning in a zigzag along the b-axis possibly increase the intermolecular overlap integral in the conducting ab-plane when they are compressed along the c-axis. If the iodine bond plays an important role in this mechanism, one can employ the iodine bond in designing new molecular conductors.

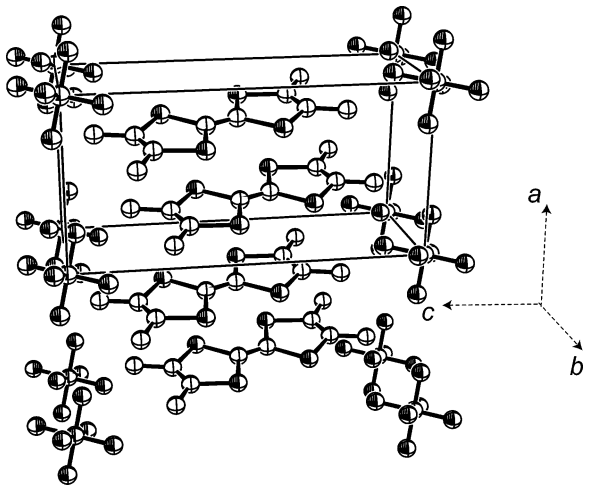

Figure 18. Crystal structure of $(TMTSF)_2PF_6$.[56]

b. $(TMTSF)_2PF_6$. $(TMTSF)_2PF_6$, discovered in 1979, is the first organic superconductor.[54,55] Its crystal structure is basically composed of TMTSF stacks parallel to the a-axis, as shown in Figure 18, which is the axis of the one-dimensional behavior of conduction electrons.[56] At ambient pressure, it shows a metal−insulator transition at about 12 K due to an instability characteristic of the one-dimensional electronic system, giving rise to spin-density waves. Hydrostatic pressures of about 0.6 GPa (6 kbar) suppressed the insulating state and induced superconductivity. Other isostructural compounds, such as $(TMTSF)_2AsF_6$ and $(TMTSF)_2TaF_6$, showed properties similar to those of the PF_6 compound but with slightly different critical pressures at which superconductivity is induced. $(TMTSF)_2ClO_4$ showed superconductivity at ambient pressure, although this compound has the anion ClO_4 that has no inversion symmetry and undergoes orientation ordering at about 24 K.[1]

It had been conjectured that hydrostatic-pressure application reduces the interstack distance and thus suppresses the one-dimensional nature of the electronic system and stabilizes the superconductivity. If this is true, uniaxial strain parallel to the b- or c-axis should induce superconductivity.

Measurements of the uniaxial strain effect on $(TMTSF)_2PF_6$ gave contradictory results:[35,57] Figure 19 shows the electrical resistance measured parallel to the one-dimensional a-axis under the uniaxial strain parallel to the same axis. Superconductivity with a T_c of 1 K was induced by the uniaxial strain under the piston pressure of about 1 GPa (10 kbar). However, insulating properties remained under the uniaxial strain parallel to the b- and c-axes induced at the same piston pressure.[58] These results can be interpreted in two ways: One is that the enhancement of the bandwidth parallel to the one-dimensional axis is important in causing superconductivity, although this idea may contradict the NMR results that suggest little change in the bandwidth when hydrostatic pressures induce superconductivity.[59,60] The other is that the uniaxial strain parallel to the a-axis not only reduces the intermolecular distance parallel to the a-axis but also modifies the intermolecular transfer integral along transverse direc-

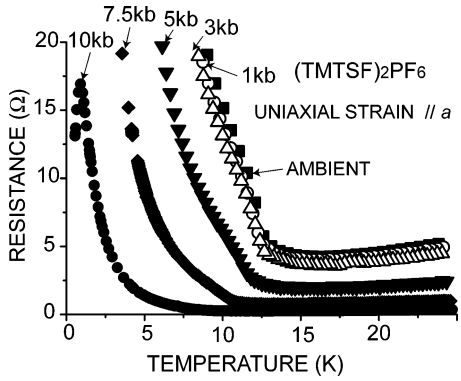

Figure 19. Electrical resistance of $(TMTSF)_2PF_6$ under the uniaxial strain parallel to the conducting a-axis created by respective piston pressure.[35,57]

tions. If this mechanism effectively increases the transverse bandwidth, one can say that the superconductivity is governed by the transverse bandwidth; that is, reduction of the one-dimensional nature is crucial for inducing superconductivity. The behavior of electrical resistivity under the piston pressure of 1 GPa (10 kbar) shown in Figure 19 reminds us of the inhomogeneous state encountered at the phase border between the spin-density-wave and superconducting states with hydrostatic pressures of about 0.6 GPa (6 kbar).[37,61,62] Both methods are considered to create the same electronic state.

A puzzling result has been obtained in the electrical resistance measured parallel to the c-axis, which is the most resistive direction, of $(TMTSF)_2PF_6$ under the uniaxial strain parallel to the c-axis. The resistance, ρ_c, decreases rapidly with increasing strain to become lower than that parallel to the one-dimensional a-axis, ρ_a, at ambient pressure.[63−65] This is surprising because ρ_c is larger than ρ_a by a factor of about 1000 at ambient pressure. There is a possibility that some dramatic structural change occurs under the above condition.

4.2. Control of Electron–Electron Coulomb Correlation

Coulomb interaction between conduction electrons prevents them from moving independently, leading to a correlation in position. This is called the Coulomb correlation. The wave function of each electron shrinks to reduce the Coulomb interaction energy due to the overlap of wave functions. A strong enough Coulomb interaction effects two features of conduction electrons: (1) The electrons lose their nature of quantum waves extending over a crystal and behave like classical particles. (2) Localized electrons form a crystal-like structure. Therefore, the Coulomb correlation makes materials insulating.[5]

The importance of the Coulomb correlation is determined by the ratio U/W or V/W, where U and V denote the Coulomb interaction energy between two electrons present on a single site or molecule and that of two electrons sitting on neighboring sites, and W denotes the conduction bandwidth. When W is much larger than U and V, electrons move with high kinetic energies that are little affected by the Coulomb interaction, and the system retains metallic properties. In the opposite case, the system is strongly correlated and shows insulating properties. When U, the on-site Coulomb energy, plays an important role, the insulating state is called the Mott insulating state. When V, the nearest-neighbor or next-nearest-neighbor interaction, in addition to U, is important, the amounts of charge on each site or molecule can be different from one another; that is, there is charge disproportionation.

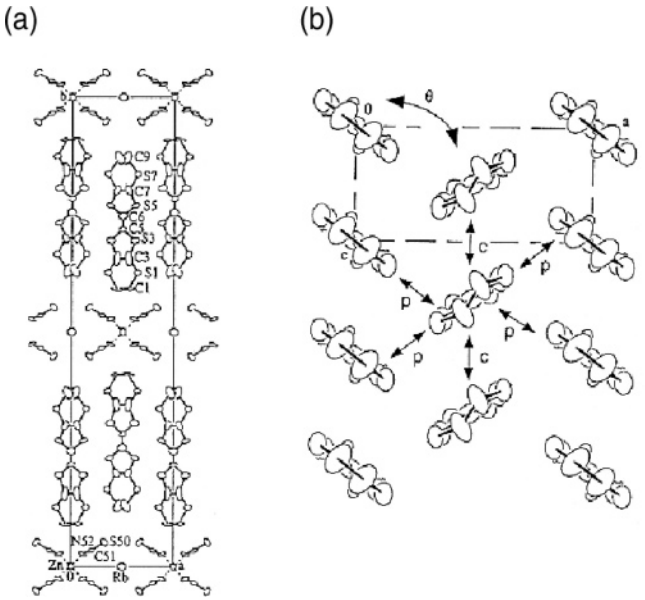

Figure 20. Crsytal structure of θ-phase BEDT-TTF conductors. (Reprinted with permission from ref 66. Copyright 1998 The American Physical Society.)

Here we describe examples of the control of the Coulomb correlation. The first example presents a modification of the Coulomb correlation through the control of the bandwidth W by the uniaxial strain. The second one shows that the Coulomb interaction U can be effectively controlled by the uniaxial strain when a suitable condition is satisfied in the crystal structure. The material of the last example has a large enough Coulomb correlation and localized electrons with spins. It will be shown that the arrangement of those spins can be modified by the uniaxial strain, allowing us to obtain novel electrical and magnetic properties.

4.2.1. Bandwidth Control and Coulomb Correlation: θ-(BEDT-TTF)$_2$CsZn(SCN)$_4$ and α-(BEDT-TTF)$_2$I$_3$

The magnitude of the Coulomb correlation, U/W or V/W, can be modified by controlling the bandwidth W. Figures 20 and 21 show the crystal structure and the phase diagram of the family of θ-phase BEDT-TTF compounds.[66] It has been suggested that the dihedral angle between neighboring BEDT-TTF molecules dominates the bandwidth of the quasi-two-dimensional conduction band formed by the layer of BEDT-TTF molecules. It has been revealed that θ-$(BEDT\text{-}TTF)_2RbZn(SCN)_4$ undergoes the Mott transition with charge disproportionation at about 250 K at ambient pressure.[67] The electrical resistance shows a sudden increase at 250 K with decreasing temperature. The CsZn compound θ-$(BEDT\text{-}TTF)_2CsZn(SCN)_4$, which has a smaller dihedral angle than

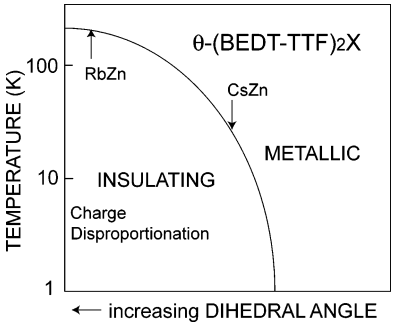

Figure 21. Phase diagram of θ-phase BEDT-TTF conductors.[66]

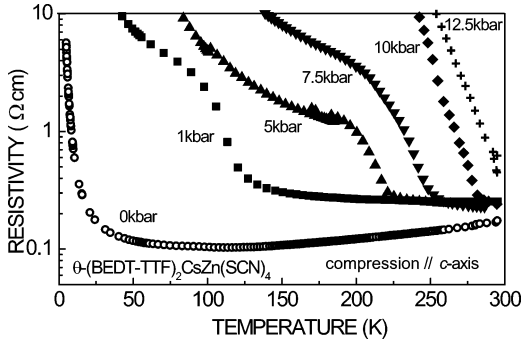

Figure 22. Electrical resistance of θ-(BEDT-TTF)$_2$CsZn(SCN)$_4$ under the uniaxial strain parallel to the c-axis.[68]

the RbZn compound, shows a gradual increase in resistance only below about 20 K. This difference between the two compounds can been ascribed to the difference in the bandwidth.

The phase diagram shown in Figure 21 suggests that uniaxial strain parallel to the c-axis of the CsZn compound enhances the insulating properties because this strain will increase the dihedral angle. Figure 22 shows the electrical resistance of θ-(BEDT-TTF)$_2$CsZn(SCN)$_4$ under the uniaxial strain parallel to the c-axis.[68] It is evident that the resistance behaves like that of the RbZn compound, as expected. It was also verified in the RbZn compound that the uniaxial strain parallel to the a-axis made it more metallic, like the CsZn compound.[69]

One may conjecture that the RbZn compound has a bandwidth narrower than that of the CsZn compound, leading to more insulating properties. X-ray structural analyses showed, however, that a tricky mechanism is in effect there.[70] The transfer integral, labeled p, along the diagonal direction suffered little change, but that parallel to the c-axis, labeled c, increased, as shown in Figure 23. One may say that the CsZn compound becomes similar to the RbZn compound under the uniaxial strain parallel to the c-axis. The total bandwidth shows no appreciable change, although the upper part of the band crossing the Fermi level is reduced and the lower part is increased by the uniaxial strain, as shown in Figure 24. This figure also shows the Fermi surfaces. The uniaxial strain makes the part of the Fermi surface perpendicular to the k_a-axis flatter, suggesting an enhanced one-dimensional nature along the a-axis. Results of theoretical studies suggest, although intuitive explanations are difficult to give, that the combination of these phenomena make the system

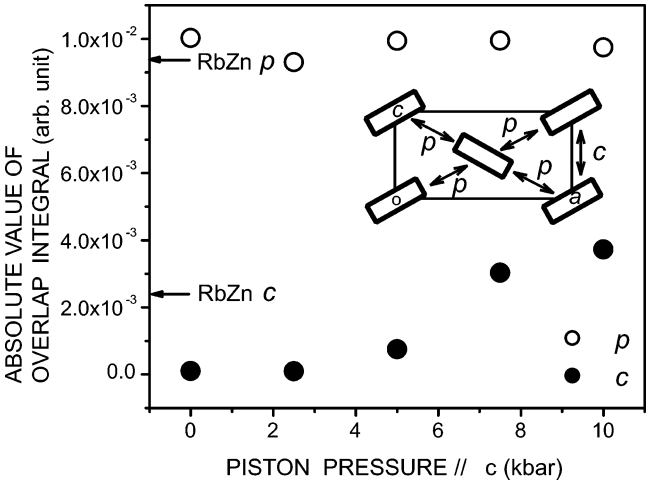

Figure 23. Transfer integral in the conducting plane of θ-(BEDT-TTF)$_2$CsZn(SCN)$_4$ with the uniaxial strain parallel to the c-axis.[70]

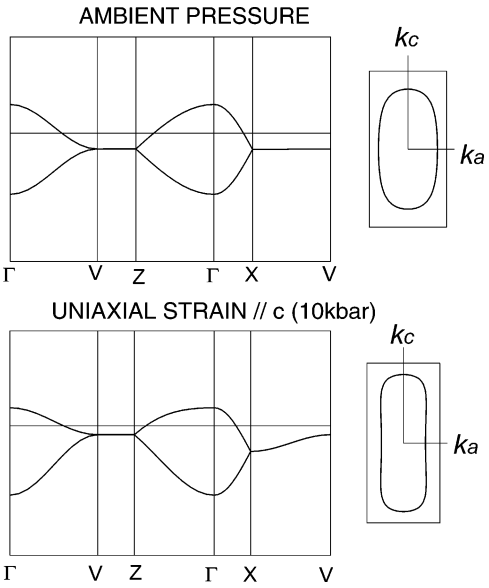

Figure 24. Band dispersion and the Fermi surface of θ-(BEDT-TTF)$_2$CsZn(SCN)$_4$ at ambient pressure and with the uniaxial strain parallel to the c-axis.[70]

more insulating, whereby charge disproportionation can take place.[71–74] One more mechanism can be pointed out for the enhancement of the Coulomb correlation. The uniaxial strain parallel to the c-axis reduces the intermolecular distance along the c-axis. This change should directly enhance the nearest-neighbor Coulomb interaction V between electrons on neighboring molecules.

α-(BEDT-TTF)$_2$I$_3$ belongs to the α-phase family of BEDT-TTF compounds. However, its electronic structure is different from that of α-(BEDT-TTF)$_2$XHg(SCN)$_4$ (X = K, NH$_4$) described in the previous section. Band calculations suggest that the Fermi surface is composed of small pockets of electrons and holes. At ambient pressure, α-(BEDT-TTF)$_2$I$_3$ shows metallic properties down to 135 K where a resistance jump occurs followed by a structural change and insulating properties.[75–77] NMR measurements have revealed that charge disproportionation occurs below 135 K.[78] The application of hydrostatic pressure causes an unusual behavior in the electrical resis-

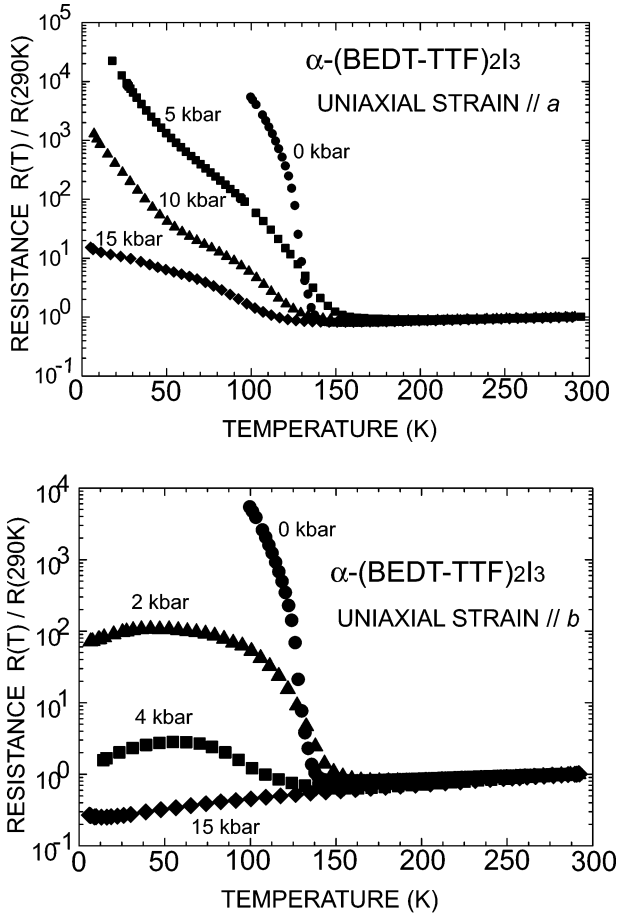

Figure 25. Electrical resistance of α-(BEDT-TTF)$_2$I$_3$ under the uniaxial strains parallel to the *a*- and *b*-axes. (Reprinted with permission from ref 22. Copyright 2000 The American Institute of Physics.)

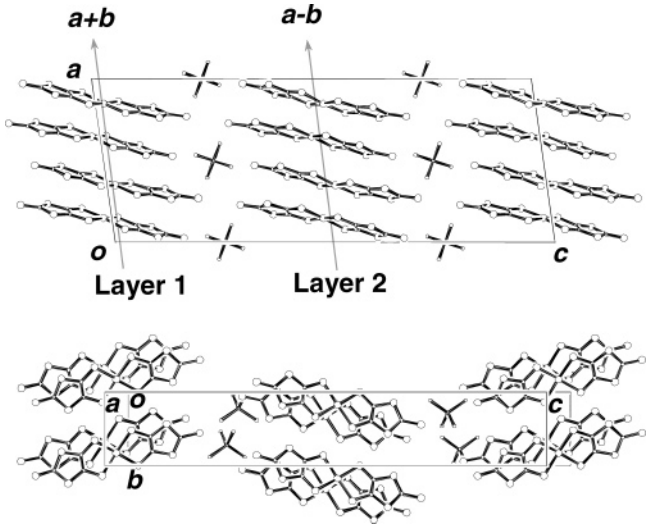

Figure 26. Crystal structure of β'-$(CH_3)_4As[Pd(dmit)_2]_2$. (Reprinted with permission from ref 85. Copyright 2002 The American Physical Society.)

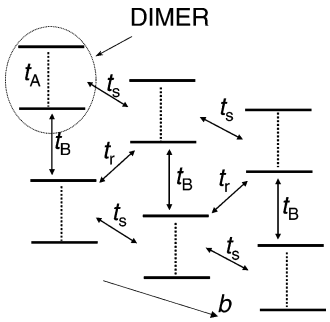

Figure 27. Crystal structure of β'-$(CH_3)_4As[Pd(dmit)_2]_2$. (Reprinted with permission from ref 85. Copyright 2002 The American Physical Society.)

tance.[79−81] The resistance shows almost no temperature dependence down to the range of 1 K. It has been suggested that the increasing mobility compensated for the decreasing number of carriers with decreasing temperature, leading to the temperature-independent resistance.[82] As shown in Figure 25, uniaxial strain parallel to the *a*-axis, which is parallel to the stacking axis of BEDT-TTF, reduced the resistance jump at 135 K and suppressed the insulating behavior, although the suppression was not complete.[22] It has been shown that superconductivity occurs at about 8 K,[83] although this has not yet been confirmed by other groups. The uniaxial strain parallel to the *b*-axis, which is in the conducting plane and nearly perpendicular to the molecular stacking axis, totally suppressed the insulating behavior, although no superconductivity was found.

X-ray measurements at both room and low temperatures under uniaxial strain clarified that the sizes of electron and hole pockets are increased and decreased by the uniaxial strain parallel to the *b*- and *a*-axes, respectively.[84] This is consistent with the results of resistance measurements, although the band calculation left some doubts about the site potential because BEDT-TTF molecules are located at two sites with slightly different symmetries.

Thus, it was found that the uniaxial strain parallel to the *b*-axis increased the bandwidth and suppressed the insulating state caused by the Coulomb correlation.

4.2.2. Control of Effective On-Site Coulomb Interaction: β'-$(CH_3)_4As[Pd(dmit)_2]_2$ and $(C_2H_5)_2(CH_3)_2N[Pd(dmit)_2]_2$

The uniaxial strain method usually modifies intermolecular transfer energies that dominate the bandwidth. However, electrical resistance measurements of β'-$(CH_3)_4As[Pd(dmit)_2]_2$, where dmit denotes 1,3-dithiol-2-thione-4,5-dithiolate, and $(C_2H_5)_2(CH_3)_2N[Pd(dmit)_2]_2$ under uniaxial strain suggested that the on-site Coulomb interaction, U, can also be effectively controlled by uniaxial strain.[85] These compounds consist of conducting layers of $Pd(dmit)_2$ molecules sandwiched by cation layers. Figure 26 shows the crystal structure of β'-$(CH_3)_4As[Pd(dmit)_2]_2$. This compound has a double layer of $Pd(dmit)_2$ separated by the cation layer. The other compound, $(C_2H_5)_2(CH_3)_2N[Pd(dmit)_2]_2$, has a single-layer structure. It is to be noted, as far as the intralayer conduction is concerned, that the conducting properties of both compounds are dominated by the triangular lattice of the $Pd(dmit)_2$ dimer, as shown in Figure 27.

The electrical conduction is driven by the charge of 0.5 electron/molecule. The dimerized structure of $Pd(dmit)_2$ molecules suggests that an effective on-site Coulomb interaction between electrons present on a single dimer, U_{dimer}, is approximated by the in-

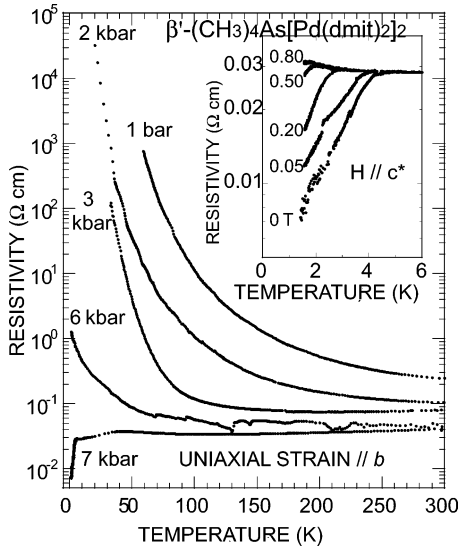

Figure 28. Electrical resistivity of β'-$(CH_3)_4As[Pd(dmit)_2]_2$ under the uniaxial strain parallel to the a-axis. (Reprinted with permission from ref 85. Copyright 2002 The American Physical Society.)

tradimer transfer energy t_A. This is because one electron occupies the bonding orbital and the other, the antibonding orbital, when U for two electrons on a single molecule is much larger than the intradimer transfer energy.

Figure 28 shows the electrical resistance of β'-$(CH_3)_4As[Pd(dmit)_2]_2$ under uniaxial strain parallel to the b-axis.[85] The uniaxial strain parallel to the b-axis stabilized the metallic state accompanied by the superconductivity below about 4 K. Uniaxial strains parallel to the a- and c-axes, however, enhanced insulating properties in the initial stage of compression, and the insulating state was never suppressed by increasing strain. The interpretation of the effect of the strain parallel to the a-axis is not straightforward because of the double-layer structure. Similar measurements were also made on $(C_2H_5)_2(CH_3)_2N[Pd(dmit)_2]_2$, which has a single-layer structure.[86] Combination of the results obtained for the two compounds has led to the following hypothesis for the roles of uniaxial strain in controlling the electronic properties of the layer of $Pd(dmit)_2$ dimers. The uniaxial strain parallel to the molecular stacking axis, the a-axis of $(C_2H_5)_2(CH_3)_2N[Pd(dmit)_2]_2$, increases the effective on-site Coulomb interaction energy on a dimer, U_{dimer}, because the increase in the intradimer transfer energy t_A enhances it. It is to be noted that the interdimer transfer energy t_B should also be increased by the uniaxial strain. It is expected, therefore, that the increase of U_{dimer} is much greater than that of the interdimer transfer energy, which leads to the more insulating state.

Measurements under hydrostatic pressure have yielded results that should be compared with those under uniaxial strain. The application of hydrostatic pressure slightly suppressed the insulating properties.[85] X-ray structural measurements under hydrostatic pressure showed that both the interdimer transfer energy and the effective on-site Coulomb energy were increased with increasing pressure and that the increase of the former was more than that of the latter, leading to a more conducting state.[87] This difference of effects between the uniaxial strain and the hydrostatic compression will be useful for future studies to modify electronic properties as desired.

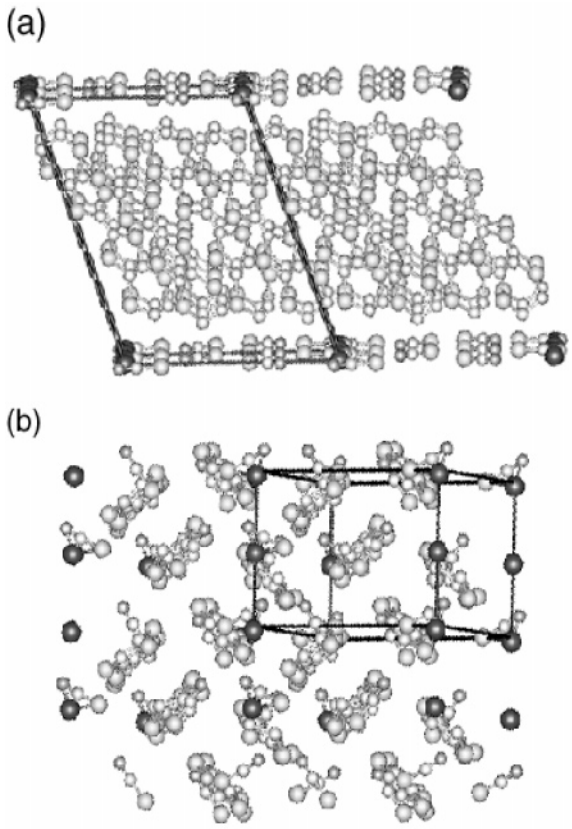

Figure 29. Crystal structure of κ-$(BEDT\text{-}TTF)_2Cu(NCS)_2$ viewed parallel to the conducting layer (a) and along the molecular long axis (b).[24]

The uniaxial strain parallel to the a+c-axis of $(C_2H_5)_2(CH_3)_2N[Pd(dmit)_2]_2$ stabilized the metallic state and led to the onset of superconductivity, because this strain increases the smallest interdimer transfer energy and results in a more regular triangular lattice of dimers, where frustration in the spin configuration is expected to suppress insulating properties due to the charge-localized state. It is noted that this effect cannot be directly observed in the double-layer compound β'-$(CH_3)_4As[Pd(dmit)_2]_2$ because the directions corrsponding to the a+c-axis of $(C_2H_5)_2(CH_3)_2N[Pd(dmit)_2]_2$ are different between the two layers. Therefore, the metallic properties of β'-$(CH_3)_4As[Pd(dmit)_2]_2$ realized under the uniaxial strain parallel to the b-axis can be ascribed to the increase of the overall bandwidth.

4.2.3. Control of Frustration in a Triangular Lattice of Spins: κ-(BEDT-TTF)$_2$X

Many molecular superconductors belong to the family of κ-$(BEDT\text{-}TTF)_2X$, where X denotes an anion such as $Cu(NCS)_2^-$.[1] Their crystals consist of conducting layers of BEDT-TTF molecules sandwiched by anion layers, as shown in Figure 29. The conducting layer is regarded as an oblique lattice of BEDT-

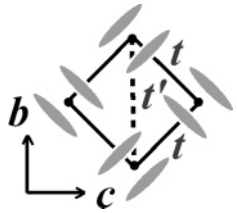

Figure 30. Schematic view of the arrangement of BEDT-TTF molecules on a conducting layer and important transfer integrals of κ-(BEDT-TTF)$_2$Cu$_2$(CN)$_3$.

TTF dimers, as shown in Figure 29b, where, on average, one hole is present on each dimer. If these charges are localized by strong on-site Coulomb interaction on each dimer, the system is in an insulating state with a spin lattice that may show some phenomena due to an ordering of the spins.

Band structure calculation suggested that the dimer lattice can be regarded as a triangular one having the frustration in the spin configuration. Figure 30 schematically shows the arrangement of BEDT-TTF molecules on the conducting layer and important transfer integrals. The band structure is described by two interdimer transfer energies, t and t'. The crystal structure at ambient pressure suggests that t' is nearly equal to t, that is, t'/t is about 1.06.

Electrical resistance measurements of κ-(BEDT-TTF)$_2$Cu$_2$(CN)$_3$ showed that the magnitude of frustration was modified by uniaxial strain.[88,89] At ambient pressure, the electrical resistance of this compound increases with decreasing temperature, suggesting a localization of conducting charges. However, magnetic susceptibility was found not to increase with decreasing temperature.[90] These properties have been ascribed to the frustration of spins localized on each dimer due to the strong on-site Coulomb interaction, that is, a Mott transition. Hydrostatic pressure of 0.06 GPa (0.6 kbar) suppresses the increase of resistance, leading to superconductivity with T_c of about 3.9 K. Under uniaxial strains parallel to both the b- and c-axes, T_c was found to increase to higher temperatures of about 7 K, as shown in Figure 31.[91] This result implies that the frustration should be suppressed by the uniaxial strain, which results in superconductivity. It is still unclear, however, how the suppression of the frustration causes the Mott insulating state to become a conducting state and what the spin configuration there is.

Also in κ-(BEDT-TTF)$_2$Cu(NCS)$_2$, the uniaxial strain effects have been studied.[92−95] The increase of T_c of 0.2−1 K was observed under the uniaxial strain parallel to the c-axis. The strain parallel to the a^*-axis reduced T_c, but one study showed an increase by about 0.1 K.[95] These effects are small compared to those of the α- and θ-phase compounds. Possible explanations for this are that (1) the bandwidth is little affected by uniaxial strains because of the dimer structure and (2) the triangular arrangement of dimers is far from the frustration because the triangle is distorted compared to that of the Cu$_2$(CN)$_3$ compound.

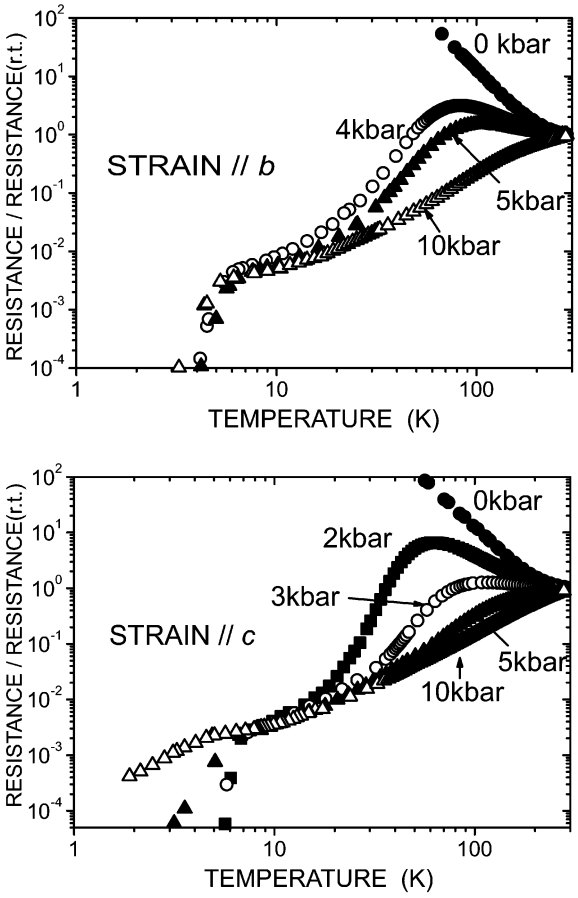

Figure 31. Electrical resistance of κ-(BEDT-TTF)$_2$Cu$_2$(CN)$_3$ under the uniaxial strains parallel to the b- and c-axes. (Reprinted with permission from ref 91. Copyright 2003 Elsevier Science.)

5. Prospect for Future Applications of Uniaxial Strain Method

Large uniaxial strains are expected to lead to more exciting electronic states. For this, one has to overcome some technical difficulties. The maximum magnitude of uniaxial strain reviewed here is about 5%, which was realized in θ-(BEDT-TTF)$_2$CsZn(SCN)$_4$. Under larger strains, crystals deteriorated, causing much broadening of X-ray diffraction peaks. The transition to the superconducting state also showed broadening of the temperature width of the transition. These are considered to be results of inhomogeneous compression of samples due to the mismatch in elastic constants between the sample and epoxy or frozen oil. For larger strains, it is necessary to search for other media with which to encase each kind of material to be studied. It is noted that such media should be solidified at or below room temperature and be chemically inactive to enable studies of organic materials.

Optical, magnetic, and some other measurements must be possible under uniaxial strains. Optical measurements in the range of visible light are expected to be possible when the piston is replaced with a transparent material such as sapphire. The pressure cell may also be replaced with a sapphire cylinder. For magnetic measurements, difficulties are similar to those under hydrostatic pressure because epoxy and frozen oil do not show great susceptibility.

It is desirable to apply the uniaxial strain method to many other materials such as conventional semiconductors and high-T_c oxide materials. For this, however, one must identify suitable pressure media that have elastic constants similar to those of the samples. Some kinds of cement may be worth testing for this purpose.

6. Summary

We have reviewed the modification and control of the electronic properties of molecular conductors and superconductors by uniaxial deformation of crystal structures. Specifically, the uniaxial strain method, where a crystal is compressed along any direction with no deformation in the transverse directions, and its application to many kinds of molecular conductors were described.

The role of pressure application in the study of molecular conductors was discussed, followed by a brief review of pioneering studies of the uniaxial compression of conventional semiconductors and some molecular conductors.

In the main text, the development of the uniaxial strain method and the novel electronic properties of molecular conductors discovered by employing the uniaxial strain method were reviewed. Examples were shown of (1) the band structure control of α-(BEDT-TTF)$_2$XHg(SCN)$_4$ (X = K, NH$_4$) to induce or enhance superconducting states, (2) the band structure modification of θ-(DIETS)$_2$[Au(CN)$_4$] and TMTSF$_2$PF$_6$ to find unexpected onsets of superconductivity, and (3) the control of effective Coulomb interaction between conducting electrons of θ-(BEDT-TTF)$_2$CsZn(SCN)$_4$, α-(BEDT-TTF)$_2$I$_3$, β'-(CH$_3$)$_4$As[Pd(dmit)$_2$]$_2$, (C$_2$H$_5$)$_2$(CH$_3$)$_2$N[Pd(dmit)$_2$]$_2$, and κ-(BEDT-TTF)$_2$X [X = Cu$_2$(CN)$_3$, Cu(NCS)$_2$]. Prospects for future studies were also given from the viewpoint of experimental methods.

7. Acknowledgments

We are grateful to T. Mori of the Tokyo Institute of Technology and M. Maesato of Kyoto University for critical reading of the manuscript and valuable advice on improving it and to R. Kato, T. Imakubo, and N. Tajima of RIKEN, H. Mori of the University of Tokyo, and K. Murata of Osaka City University for providing original experimental data to prepare some of the figures presented here. We thank J. S. Brooks of Florida State University, K. Kajita of Toho University, T. Ishiguro of Doshisha University, K. Kanoda of the Univeisity of Tokyo, H. Ito of Nagoya University, H. Seo and M. Tokumoto of the National Institute of Advanced Industrial Science and Technology, Japan, C. Hotta of Aoyama Gakuin University, and the scientists named above for illuminating discussions. We also thank the authors and publishers of papers for permission to reproduce their figures in this review.

8. References

(1) For a review, see, for example: Ishiguro, T.; Yamaji, K.; Saito, G. *Organic Superconductors*; Springer: Berlin, Germany, 1998.
(2) Kino, H.; Fukuyama, H. *J. Phys. Soc. Jpn.* **1995**, *64*, 1877.
(3) Kanoda, K. *Physica C* **1997**, *282−287*, 299.
(4) Kanoda, K. *Hyperfine Int.* **1997**, *104*, 235.
(5) Seo, H.; Hotta, C.; Fukuyama, H. *Chem Rev.*
(6) As a review, see: Cardona, M. *Phys. Status Solidi B* **1996**, *198*, 5.
(7) Leroux, M.; Gil, B. *Ann. Phys. −Paris* **1995**, *20*, 109.
(8) Baidakov, V. V.; Ermakov, V. N.; Gorin, A. E.; Kolomoets, V. V.; Shenderovskii, V. A. *J. Phys. Chem. Solids* **1995**, *56*, 319.
(9) Welp, U.; Grimsditch, M.; Fleshler, S.; Nessler, W.; Downey, J.; Crabtree, G. W. *Phys. Rev. Lett.* **1992**, *69*, 2130.
(10) Sanfilippo, S.; Beille, J.; Pourtier, F.; Villegier, C.; Chateigner, D.; Germi, P.; Pernet, M.; Noel, H. *Solid State Commun.* **1995**, *96*, 391.
(11) Meingast, C.; Jilek, E.; Kaldis, E. *Physica C* **1993**, *209*, 591.
(12) Belensky, G. L.; Greene, S. M.; Roytburd, A.; Lobb, C. J.; Hagen, S. J.; Greene, R. L. *Phys. Rev. B* **1991**, *44*, 10117.
(13) Jones, G.; Dunstan, D. J. *Rev. Sci. Instrum.* **1996**, *67*, 489.
(14) Ves, S.; Cardona, M. *Solid State Commun.* **1981**, *38*, 1109.
(15) Greene, R. L.; Street, G. B.; Suter, L. J. *Phys. Rev. Lett.* **1975**, *34*, 577.
(16) Chiang, C. K.; Heeger, A. J.; MacDiarmid, A. G. *Phys. Lett.* **1977**, *60A*, 375.
(17) Davidson, A. T.; Yoffe, A. D. *Philos. Mag.* **1977**, *36*, 1083.
(18) Bouffard, S.; Zuppiroli, L. *Solid State Commun.* **1978**, *28*, 113.
(19) Tokumoto, M.; Murata, K.; Kinoshita, N.; Yamaji, K.; Anzai, H.; Tanaka, Y.; Hayakawa, Y.; Nagasaka, K.; Sugawara, Y. *Mol. Cryst. Liq. Cryst.* **1990**, *181*, 295.
(20) Kusuhara, H.; Sakata, Y.; Ueba, Y.; Tada, K.; Kaji, M.; Ishiguro, T. *Solid State Commun.* **1990**, *74*, 251.
(21) Campos, C. E.; Brooks, J. S.; van Bentrum, P. J. M.; Perenboom, J. A. A.; Rook, J.; Klepper, S. J.; Tokumoto, M. *Rev. Sci. Instrum.* **1995**, *66*, 1061.
(22) Maesato, M.; Kaga, Y.; Kondo, R.; Kagoshima, S. *Rev. Sci. Instrum.* **2000**, *71*, 176.
(23) Ishiguro, T.; Kagoshima, S.; Anzai, H. *J. Phys. Soc. Jpn.* **1977**, *42*, 365.
(24) Mori, H.; Tanaka, S.; Oshima, M.; Saito, G.; Mori, T.; Maruyama, Y.; Inokuchi, H. *Bull. Chem. Soc. Jpn.* **1990**, *63*, 2183.
(25) Mori, T.; Inokuchi, H.; Mori, H.; Tanaka, S.; Oshima, M.; Saito, G. *J. Phys. Soc. Jpn.* **1990**, *59*, 2624.
(26) Wang, H. H.; Carlson, K. D.; Geiser, U.; Kwok, W. K.; Vashon, M. D.; Thompson, J. E.; Larsen, N. F.; McCabe, G. D.; Hulscher, R. S.; Williams, J. M. *Physica C* **1990**, *166*, 57.
(27) Mori, H.; Tanaka, S.; Oshima, K.; Saito, G.; Mori, T.; Maruyama, Y.; Inokuchi, H. *Solid State Commun.* **1990**, *74*, 1261.
(28) Sasaki, T.; Toyota, N.; Tokumoto, M.; Kinoshita, N.; Anzai, H. *Solid State Commun.* **1990**, *75*, 93
(29) Kinoshita, N.; Tokumoto, M.; Anzai, H. *J. Phys. Soc. Jpn.* **1990**, *60*, 2131.
(30) Kushch, N. D.; Buravov, L. I.; Kartsovnik, M. V.; Laukhin, V. N.; Pesotskii, S. J.; Shibaeva, R. P.; Rozenberg, L. P.; Yagubskii, E. B.; Zvarikina, A. V. *Synth. Met.* **1992**, *46*, 271.
(31) Kartsovnik, M. V.; Kovalev, A. E.; Kushch, N. D. *J. Phys. I (Paris)* **1993**, *3*, 1187.
(32) Kouno, T.; Osada, T.; Hasumi, M.; Kagoshima, S.; Miura, N.; Oshima, M.; Mori, H.; Nakamura, T.; Saito, G. *Synth. Met.* **1993**, *55−57*, 2425.
(33) Hanasaki, N.; Kagoshima, S.; Miura, N.; Saito, G. *J. Phys. Soc. Jpn.* **1996**, *65*, 1010.
(34) Maesato, M.; Kaga, Y.; Kondo, R.; Kagoshima, S. *Phys. Rev. B* **2001**, *64*, 155104.
(35) Kagoshima, S.; Kondo, R.; Hirai, H.; Shibata, T.; Kaga, Y.; Maesato, M. *Phys. Status Solidi B* **2001**, *223*, 97.
(36) Kagoshima, S.; Shibata, T.; Hirai, H.; Kondo, R.; Maesato, M. *Curr. Appl. Phys.* **2001**, *1*, 72.
(37) Greene, R. L.; Engler, E. M. *Phys. Rev. Lett.* **1980**, *45*, 1587.
(38) Andres, K.; Wudl, F.; McWhan, D. B.; Thomas, G. A.; Nalewajek, D.; Stevens, A. L. *Phys. Rev. Lett.* **1980**, *45*, 1449.
(39) Shultz, H. J.; Jérome, D.; Ribault, M.; Mazaud, A.; Bechgaard, K. *J. Phys. (Paris)* **1982**, *43*, 801.
(40) Laukhin, V. N.; Kostyuchenko, E. E.; Sushko, Yu. V.; Shchegolev, J. F.; Yagubskii, E. B. *JETP Lett.* **1985**, *41*, 81.
(41) Murata, K.; Tokumoto, M.; Anzai, H.; Bando, H.; Saito, G.; Kajimura, K.; Ishiguro, T. *J. Phys. Soc. Jpn.* **1985**, *54*, 2084.
(42) Murata, K.; Honda, Y.; Anzai, H.; Tokumot, H.; Takahashi, K.; Kinoshita, N.; Ishiguro, T. *Synth. Met.* **1989**, *27*, A263.
(43) Mori, N. *The Physics and Chemistry of Oxide Superconductors*; Iye, Y., Yasuoka, H., Eds.; Springer-Verlag: Berlin, Germany, 1992; 191 pp.
(44) For a review, see, for example: Singleton, J. *Rep. Prog. Phys.* **2000**, *63*, 1111.
(45) Kagoshima, S.; Maesato, M.; Kondo, R.; Shibata, T.; Hirai, H. *Synth. Met.* **2001**, *120*, 683.
(46) Kagoshima, S.; Kondo, R.; Maesato, M. *Curr. Appl. Phys.* **2001**, *1*, 307.
(47) Kondo, R.; Kagoshima, S.; Maesato, M. *Phys. Rev. B* **2003**, *67*, 134519.

(48) Rousseau, R.; Doublet, M.-L.; Canadell, E.; Shibaeva, R. P.; Khasanov, S. S.; Rozenberg, L. P.; Kushch, N. D.; Yagubskii, E. B. *J. Phys. I Fr.* **1996**, *6*, 1527.
(49) Imakubo, T.; Tajima, N.; Tamura, M.; Kato, R.; Nishio, Y.; Kajita, K. *J. Mater. Chem.* **2002**, *12*, 159.
(50) Imakubo, T.; Tajima, N.; Tamura, M.; Kato, R.; Nishio, Y.; Kajita, K. *Synth. Met.* **2003**, *133*−*134*, 159.
(51) Metrangolo, P.; Resnati, G. *Chem. Eur. J.* **2001**, *7*, 2511, and references cited therein.
(52) Yamada, J.; Sugimoto, T. *TTF Chemistry: Fundamentals and Applications of Tetrathiafulvalene*; Kodansha: Tokyo, Japan, 2004.
(53) Tajima, N.; Imakubo, T.; Kato, R.; Nishio, Y.; Kajita, K. *J. Phys. Soc. Jpn.* **2003**, *72*, 1014.
(54) Bechgaard, K.; Jacobsen, C. S.; Mortensen, K.; Pedersen, J. H.; Thorup, N. *Solid State Commun.* **1980**, *33*, 1119.
(55) Jérome, D.; Mazaud, A.; Ribault, M.; Bechgaard, K. *J. Phys. Lett.* **1980**, *41*, L95.
(56) Thorup, N.; Rindorf, G.; Soling, H.; Bechgaard, K. *Acta Crystallogr. B* **1981**, *37*, 1236.
(57) Kagoshima, S.; Maesato, M.; Kondo, R.; Shibata, T.; Hirai, H. *Synth. Met.* **2001**, *120*, 683.
(58) Guo, F.; Murata, K.; Oda, A.; Yoshino, H. *J. Phys. Soc. Jpn.* **2000**, *69*, 2164.
(59) Miyazaki, M.; Kishigi, K.; Hasegawa, Y. *J. Phys. Soc. Jpn.* **2000**, *69*, 997.
(60) Takahashi, T.; Kawamura, H.; Ohyama, T.; Maniwa, Y.; Murata K. *J. Phys. Soc. Jpn.* **1989**, *58*, 703.
(61) As a review, see, for example: Jérome, D. *Mol. Cryst. Liq. Cryst.* **1982**, *79*, 155.
(62) Brusetti, R.; Jérome, D.; Ribault, M.; Bechgaard, K. *J. Phys. (Paris)* **1982**, *43*, 801.
(63) Murata, K.; Mizuno, Y.; Guo, F. Z.; Shodai, S.; Iwashita, K.; Yoshino, H. *Mol. Cryst. Liq. Cryst.* **2002**, *380*, 85.
(64) Murata, K.; Iwashita, K.; Mizuno, Y.; Guo, F. Z.; Shodai, S.; Yoshino, H.; Brooks, J. S.; Balicas, L.; Graf, D.; Storr, K.; Rutel, I.; Uji, S.; Terakura, C.; Imanaka, Y. *Synth. Met.* **2003**, *133*, 51.
(65) Murata, K.; Iwashita, K.; Mizuno, Y.; Guo, F. Z.; Shodai, S.; Yoshino, H.; Brooks, J. S.; Balicas, L.; Graf, D.; Storr, K.; Rutel, I.; Uji, S.; Terakura, C.; Imanaka, Y. *J. Phys. Chem. Solids* **2002**, *63*, 1263.
(66) Mori, H.; Tanaka, S.; Mori, T. *Phys. Rev. B* **1998**, *57*, 12023.
(67) Miyagawa, K.; Kawamoto, A.; Kanoda, K. *Phys. Rev. B* **2000**, *62*, 7679.
(68) Kondo, R.; Kagoshima, S.; Chusho, M.; Hoshino, H.; Mori, T.; Mori, H.; Tanaka, S. *Curr. Appl. Phys.* **2002**, *2*, 483.
(69) Iwashita, K.; Yamamoto, H. M.; Yoshino, H.; Graf, D.; Storr, K.; Rutel, I.; Brooks, J. S.; Takahashi, T.; Murata K. *Synth. Met.* **2003**, *133*−*134*, 153.
(70) Kondo, R.; Higa, M.; Kagoshima, S.; Hoshino, H.; Mori, T.; Mori, H. *Curr. Appl. Phys.* **2004**, *4*.
(71) Seo, H. *J. Phys. Soc. Jpn.* **2000**, *69*, 805.
(72) Mori, T. *Bull. Chem. Soc. Jpn.* **2000**, *73*, 2243.
(73) Mori, T. *J. Phys. Soc. Jpn.* **2003**, *72*, 1469.
(74) Hotta, C. *J. Phys. Soc. Jpn.* **2003**, *72*, 840
(75) Nogami, Y.; Kagoshima, S.; Sugano, T.; Saito, G. *Synth. Met.* **1986**, *16*, 367.
(76) Bender, K.; Henning, I.; Schweitzer, D.; Dietz, K.; Endres, H.; Keller, H. *Mol. Cryst. Liq. Cryst.* **1984**, *108*, 359.
(77) Bender, K.: Dietz, K.; Endres, H.; Helberg, H. W.; Henning, I.; Keller, H. J.; Schafer, H. W.; Schweitzer, D. *Mol. Cryst. Liq. Cryst.* **1984**, *107*, 45.
(78) Takano, Y.; Hiraki, K.; Yamamoto, H. M.; Nakamura, T.; Takahashi, T. *J. Phys. Chem. Sol.* **2001**, *62*, 393.
(79) Kajita, K.; Ojiro, T.; Fujii, H.; Nishio, Y.; Kobayashi, H.; Kobayashi, A.; Kato, R. *J. Phys. Soc. Jpn.* **1992**, *61*, 23.
(80) Ojiro, T.; Kajita, K.; Nishio, Y.; Kobayashi, H.; Kobayashi, A.; Kato, R.; Iye, Y. *Physica B* **1993**, *184*, 494.
(81) Tajima, N.; Tajima, A.; Tamura, M.; Nishio, Y.; Kajita, K. *Synth. Met.* **2003**, *133*−*134*, 147.
(82) Tajima, N.; Tamura, M.; Nishio, Y.; Kajita, K.; Iye, Y. *J. Phys. Soc. Jpn.* **2000**, *69*, 543.
(83) Tajima, N.; Eniba-Tajima, A.; Tamura, M.; Nishio, Y.; Kajita, K. *J. Phys. Soc. Jpn.* **2002**, *71*, 1832.
(84) Kondo, R.; Kagoshima, S. *J. Phys. C* **2004**.
(85) Kato, R.; Tajima, N.; Tamura, M.; Yamaura, J. *Phys. Rev. B* **2002**, *66*, 020508.
(86) Kato, R.; Tajima, A.; Tajima, N.; Tamura, M. *J. Phys. C* **2004**.
(87) Yamaura, J.-I.; Nakao, A.; Kato, R. *J. Phys. Soc. Jpn.* **2004**, *73*.
(88) Maesato, M.; Shimizu, Y.; Ishikawa, T.; Saito, G. *Synth. Met.* **2003**, *137*, 1243.
(89) Maesato, M.; Shimizu, Y.; Ishikawa, T.; Saito, G. *J. Phys. C* **2004**.
(90) Shimizu, Y.; Maesato, M.; Saito, G.; Miyagawa, K.; Kanoda, K. *Phys. Rev. Lett.* **2003**, *91*, 107001.
(91) Shimizu, Y.; Maesato, M.; Saito, G.; Drozdova, O.; Ouahab, L. *Synth. Met.* **2003**, *133*−*134*, 225.
(92) Tokumoto, M.; Mizutani, T.; Kinoshita, T.; Brooks, J. S.; Uwatoko, Y.; Drozdova, O.; Yakushi, K.; Tamura, I.; Kobayashi, H.; Mangetsu, T.; Yamada, J.; Ishida, K. *Mol. Cryst. Liq. Cryst.* **2002**, *380*, 227.
(93) Mizutani, T.; Tokumoto, M.; Kinoshita, T.; Brooks, J. S.; Uwatoko, Y.; Drozdova, O.; Yakushi, K.; Tamura, I.; Kobayashi, H.; Mangetsu, T.; Yamada, J.; Ishida, K. *Synth. Met.* **2003**, *133*−*134*, 229.
(94) Ishikawa, T.; Maesato, M.; Saito, G. *Synth. Met.* **2003**, *133*−*134*, 227.
(95) Ito, H.; Hasegawa, Y.; Ishida, A.; Takasaki, S.; Yamada, J.; Anzai, H. *Synth. Met.* **2003**, *133*−*134*, 233.

CR0306539